# Theoretical study of Ziegler–Natta olefin polymerization mechanisms on heterogeneous catalysts and on homogeneous catalysts by using "PIO" analysis and "LFO" calculation

Akinobu Shiga and Masaaki Kubota

*Tsukuba Rsearch Laboratory, Sumitomo-Chemical Co., Ltd., 6 Kitahara, Tsukuba 300-32, Japan*

Received 12 June 1997; accepted 11 August 1997

Polymerization mechanisms on $O_h$-propyltitaniumchlorides and $T_d$-propyltitaniumchlorides, active site models of $TiCl_3$ catalysts and metallocene catalysts, respectively, are studied by using "paired interacting orbitals" (PIO) analysis and "localized frontier orbitals" (LFO) calculation. In the case of $TiCl_3$ catalysts the possible route of an incoming ethylene is constrained by Cl anions located in the ethylene insertion plane. In the case of metallocene catalysts, such a constraint does not appear, and therefore, they should be superior to $TiCl_3$ catalysts in catalytic activity. The low reactivities of $TiCl_3$ catalysts are removed considerably by making $Ti_{2n}$ clusters on the crystalline surface.

**Keywords:** Ziegler catalysts, metallocene catalysts, olefin polymerization, MO calculations, orbitals interaction

## 1. Introduction

One of the most important discoveries in this century in chemistry and chemical industries is the Ziegler–Natta catalysts for polymerization of olefins. The highly active heterogeneous catalysts have modernized the poly-olefins manufacturing processes and now gas phase processes are becoming the main stream of new production technologies. Since the discovery of highly active homogeneous metallocene catalysts by Kaminsky et al. [1], much interest has been directed to homogeneous catalysts, because of their possibilities of producing versatile polymers: syndiotactic polypropylene, syndiotactic polystyrene, ethylene/olefin copolymer with very sharp molecular weight distribution etc. Nowadays, the needs of catalysts which enable to control molecular weight and its distribution, copolymerization ratio, regio- and stereo-selectivities, and so on, are increasing more to produce polymers with desirable chemical and physical properties. It is important to know the factors that play crucial roles in the polymerization procedure. It may be especially useful to know the difference between the polymerization mechanism on heterogeneous catalysts and that on homogeneous catalysts in order to develop such sophisticated catalysts.

The Cossee mechanism has widely been accepted as the most plausible for the Ziegler–Natta polymerization mechanism [2]. The mechanism is as follows. The active site is a metal alkyl and the olefin coordinates to the vacancy of the metal alkyl in forming a $\pi$-complex. The olefin inserts then into the metal–alkyl bond through a four-membered cyclic transition state, and these processes are repeated. Many theoretical studies on the polymerization processes have been reported. Novaro et al. [3] first studied the ethylene insertion in the Cossee mechanism by means of ab initio RHF calculations to verify the concerted motion that had been proposed by Armstrong et al. [4], and to estimate the activation energy roughly to be 15 kcal/mol. Jolly and Marynick reported the direct insertion of ethylene in the real metallocene initiator system, $[Cp_2TiCH_3]^+$ [5]. The activation energy was 9.8 kcal/mol, using ab initio calculations with MP2 level corrections.

Recent developments in ab initio MO computational methods make it possible to determine the energetics of a full catalytic cycle. Kawamura et al. [6] studied the mechanism of the insertion of ethylene and propylene into $[Cl_2TiCH_3]^+$ and determined the structures and energies of the reactants, the $\pi$-complex, the transition state and the product. They found that the activation energy is about 4 kcal/mol with DPUMP2 level corrections, the barrier of propylene insertion being higher than that of ethylene insertion, and the primary insertion being easier than the secondary. Yoshida et al. [7] studied the repetitive insertion of ethylene into the metal–alkyl bond and the $\beta$-H elimination, which is considered to be a chain-transfer step, in $[H_2SiCp_2MCH_3]^+$ (M = Ti, Zr, Hf)/ethylene systems. All the stationary structures were optimized at the RHF level and the energetics was obtained at the RQCISD level. They reported that the activation energy of the ethylene insertion is 7–10 kcal/mol and the isomerization of $\gamma$-H agostic product to the more stable $\beta$-H agostic propyl complex requires a high activation energy. It has also been reported that the $\beta$-H elimination from the $\beta$-H agostic propyl complex is endothermic by about 50 kcal/mol and takes place with difficulty.

A density functional study on the insertion and chain

termination of ethylene with $[Cp_2ZrCH_2CH_3]^+$ has been reported by Lohrenz et al. [8]. There are two directions of the incoming ethylene. The frontside insertion of the incoming ethylene to the $\beta$-H agostic $[Cp_2ZrCH_2CH_3]^+$ takes place with the rotation around the Zr–$C_\alpha$ bond leading to the $\alpha$-H agostic $[Cp_2ZrCH_2CH_3]^+$. When the rotation does not occur, a $\pi$-complex is formed and a hydrogen transfer from the end of the polymer chain to the ethylene takes place. Another one is a backside insertion. Among three chain termination processes ($\beta$-H elimination, C–H activation, and H-exchange), H-exchange is the most probable one.

Ab initio calculations of more real metallocene catalysts seem to be in progress [9].

The requirement of a powerful method for analysing the calculated results and predicting the catalytic activities will increase as the catalysts become larger in size. Fujimoto et al. [10] proposed a method of determining unequivocally the orbitals which should play dominant roles in chemical interactions between two systems. Interactions were represented compactly in terms of a few pairs of localized orbitals. In each orbital pair, one orbital belongs to one fragment species, that is a catalyst, and the other orbitals to the other fragment species, that is a reactant. They called those orbitals "paired interacting orbitals" (PIO). Although this analysis was proposed originally for ab initio calculations, we reported that this approach was also useful in analysing the results of extended Hückel calculations [11]. By applying the PIO analysis to olefin insertion in several models of Ziegler–Natta catalytic systems, including $TiCl_3$ crystalline surface, it has been clarified that electron delocalization from olefin to the catalytic site and that from catalytic site to olefin play a crucial role in olefin insertion. The former depends on electrophilicity of the active site and the latter on nucleophilicity of the active site. Fujimoto et al. [12] also proposed the way of estimating the electrophilicity and nucleophilicity of reaction sites based on electron delocalization. By using this method, we predicted the reactivities of ethylene insertion into the Ti–methyl bond in $d^0$ methyltitanium complexes [13].

Most of the theoretical studies have been done assuming the model of a homogeneous catalyst in which an active site has a tetrahedral ($T_d$) structure. Another important type of catalyst is a heterogeneous one, a $TiCl_3$ type or a supported type catalyst. The active site of the heterogeneous catalyst has an octahedral ($O_h$) structure.

In this paper, we study the insertion of ethylene and the chain termination adopting a model of heterogeneous Ziegler–Natta catalysts and clarify the effects of the shape of the active site of olefin polymerization catalysts. This study consists of three parts: (1) investigation of the active site on the $TiCl_3$ crystalline surface, (2) the direction of ethylene coordination to the $\beta$-H agostic propyltitanium complex, frontside or backside, (3) the ethylene insertion in $d^1$ propyltitanium complexes.

## 2. Method

### 2.1. Ab initio calculation

We used the restricted Hartree–Fock energy gradient technique of GAUSSIAN 94 for the geometry optimization [14]. The basis functions used for Ti were MIDI4 of Huzinaga et al. [15] for the $^5F$ state, which were augmented by two sets of valence p functions (exponent = 0.083 and 0.028) with the overall split-valence contraction (43321/4311/31). For C, H, and Cl atoms we used the 3-21G basis functons [16].

### 2.2. PIO analysis

We divide a model complex (combined system C) into two fragments, [A] and [B] as shown figure 1. The geometries of [A] and [B] were the same as those in the original complex ([A+B] ≡ [C]).

The molecular orbitals of [A], [B] and [C] were calculated by the extended Hückel method [17]. The extended Hückel parameters are given in the appendix. PIOs were obtained by applying the procedure that was proposed by Fujimoto et al. [10].

The procedure is summarized as follows:

(1) We expand the MOs of a complex in terms of the MOs of two fragment species, by determining the expansion coefficients $c_{i,f}$, $c_{m+j,f}$ and $d_{k,f}$, $d_{n+l,f}$:

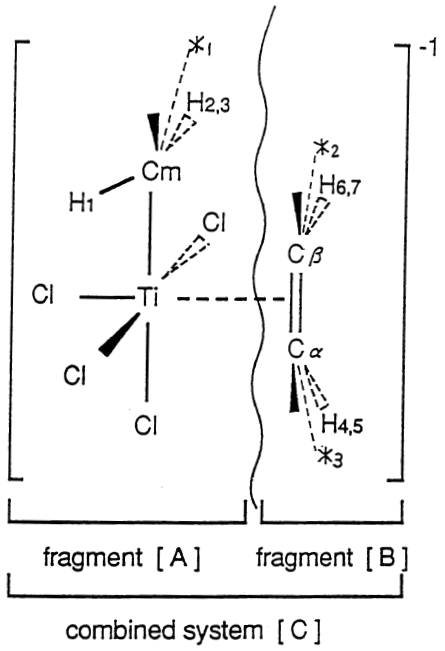


Figure 1. Schematic illustration of the combined system, and fragments [A] and [B].

$$\Phi_f = \sum_{i=1}^{m} c_{i,f}\phi_i + \sum_{j=1}^{M-m} c_{m+j,f}\phi_{m+j} + \sum_{k=1}^{n} d_{k,f}\psi_k + \sum_{l=1}^{N-n} d_{n+l,f}\psi_{n+l}\,,$$

$$f = 1, 2, \ldots, m+n\,, \tag{1}$$

where $\Phi$ are MOs of the complex [C], $\phi$ and $\psi$ are the MOs of the fragments [A] and [B] respectively, $m$ and $n$ indicate the number of occupied MOs of A and B, respectively, and $M$ and $N$ represent the number of basis functions of A and B, respectively.

(2) We construct an interaction matrix $\mathcal{P}$ which represents the interaction between the MOs of the fragment [A] and the MOs of the fragment [B]:

$$\mathcal{P} = \begin{pmatrix} P_{i,k} & P_{i,n+1} \\ P_{m+j,k} & P_{m+j,n+1} \end{pmatrix}, \tag{2}$$

in which

$$P_{i,k} = 2\sum_{f=1}^{m+n} c_{i,f}d_{k,f} \qquad i = 1 \sim m, k = 1 \sim n\,,$$

$$P_{i,n+1} = 2\sum_{f=1}^{m+n} c_{i,f}d_{n+l,f} \qquad i = 1 \sim m, l = 1 \sim N-n\,,$$

$$P_{m+j,k} = 2\sum_{f=1}^{m+n} c_{m+j,f}d_{k,f} \qquad j = 1 \sim M-m, k = 1 \sim 1-n\,,$$

$$P_{m+j,n+1} = 2\sum_{f=1}^{m+n} c_{m+j,f}d_{n+l,f} \qquad j = 1 \sim M-m, l = 1 \sim N-n\,.$$

(3) We obtain transformation matrices $\mathcal{U}^{\mathrm{A}}$ (for A) and $\mathcal{U}^{\mathrm{B}}$ (for B) by

$$\mathcal{P}^{\dagger}\mathcal{P}\mathcal{U}^{\mathrm{A}} = \mathcal{U}^{\mathrm{A}}\gamma\,, \tag{3}$$

$$\mathcal{U}^{\mathrm{B}}_{s,v} = (\gamma_v)^{-1/2}\Sigma_r^N P_{r,s}\mathcal{U}^{\mathrm{A}}_{r,v} \quad (v = 1, 2, \ldots, N)\,. \tag{4}$$

(4) Finally we calculate the PIOs by

$$\phi'_v = \Sigma_r^N U^{\mathrm{A}}_{r,v}\phi_r \quad (\text{for A})\,, \tag{5}$$

$$\psi'_v = \Sigma_s^N U^{\mathrm{B}}_{s,v}\psi_s \quad (\text{for B})\,. \tag{6}$$

The $N \times M$ ($N \leqslant M$) orbital interactions in the complex C can thus be reduced to the interactions of $N$ PIOs, $N$ indicating the smaller of the numbers of MOs of the two fragments, A and B.

PIO calculations were carried out on an LUMMOX system with NEC PC-9801RA [18].

### 2.3. LFO energy calculation

LFO energies were calculated according to the procedure proposed by Fujimoto et al. [12]. The reference orbital, which is determined by PIO analysis, denoted here by $\delta_r$ can be expanded in terms of the occupied MOs $\phi_i$ and the unoccupied MOs $\phi_j$ of a propyltitanium complex (A):

$$\delta_r = \sum_i^{\mathrm{oc}} d_{i,r}\phi_i + \sum_j^{\mathrm{unoc}} d_{j,r}\phi_j\,. \tag{7}$$

Then, the occupied and unoccupied orbital that are the closest to $\delta_r$ are respectively defined by

$$\phi_{\mathrm{oc}}(\delta_r) = \left(\sum_i^{\mathrm{oc}} d_{i,r}\phi_i\right) \Big/ \left(\sum_i^{\mathrm{oc}} d_{i,r}^2\right)^{1/2}, \tag{8}$$

$$\phi_{\mathrm{unoc}}(\delta_r) = \left(\sum_j^{\mathrm{unoc}} d_{j,r}\phi_j\right) \Big/ \left(\sum_j^{\mathrm{unoc}} d_{j,r}^2\right)^{1/2}. \tag{9}$$

These orbitals are given by a linear combination of the occupied and unoccupied canonical MOs, respectively, and, therefore, the electron-donating or -accepting strength is evaluated by

$$\lambda_{\mathrm{oc}}(\delta_r) = \left(\sum_i^{\mathrm{oc}} d_{j,r}^2\epsilon_i\right) \Big/ \left(\sum_i^{\mathrm{oc}} d_{j,r}^2\right), \tag{10}$$

$$\lambda_{\mathrm{unoc}}(\delta_r) = \left(\sum_j^{\mathrm{unoc}} d_{j,r}^2\epsilon_j\right) \Big/ \left(\sum_j^{\mathrm{unoc}} d_{j,r}^2\right), \tag{11}$$

where $\epsilon_i$ and $\epsilon_j$ are the orbital energies of the component MOs $\phi_i$ and $\phi_j$. With the same procedure as described above, we can obtain the electron-donating and -accepting strength of the ethylene molecule (B).

Then, a reactivity index (RI) is defined by

$$\mathrm{RI} = 1/(\lambda_{\mathrm{A\,unoc}} - \lambda_{\mathrm{B\,oc}}) + 1/(\lambda_{\mathrm{B\,unoc}} - \lambda_{\mathrm{A\,oc}})\,. \tag{12}$$

The first term on the right-hand side estimates the magnitude of electron delocalization from ethylene molecule (B) to the propyltitanium complex (A) and the second term estimates that from A to B.

## 3. Results and discussion

### 3.1. An active site model on the $TiCl_3$ crystalline surface

Many kinetic, morphological, and crystallographic studies of heterogeneous polymerization catalysts [19] have revealed that the violet $TiCl_3$ crystal consists of stacks of elementary crystal sheets, each of which contains two chlorine layers with one titanium layer between them, and the precursor of an active site is located on the edge of the basal face of violet $TiCl_3$ crystalline surface. The precursor has a Cl vacancy and a dangling bonded Cl atom which is alkylated by an alkylaluminum co-catalyst to form the active site. Figure 2 shows the structure of a $CH_3Ti_{16}Cl_{47}$ cluster which has been cut from an edge of the basal face of the violet $TiCl_3$ crystalline. Pairs of

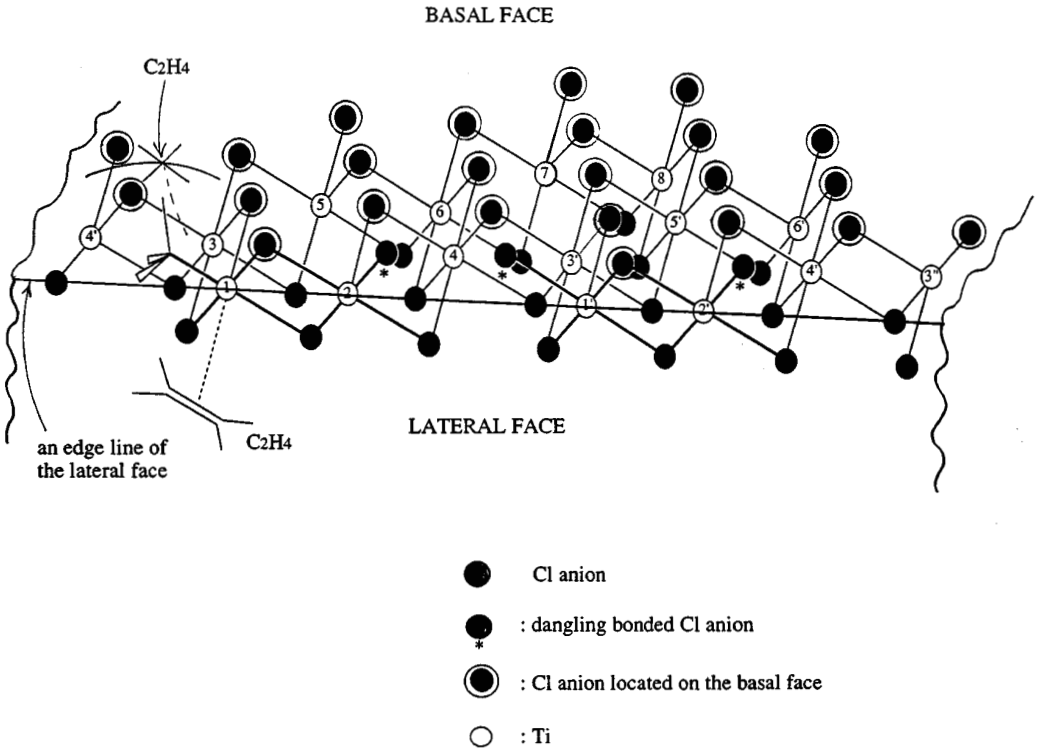


Figure 2. $CH_3Ti_{16}Cl_{47}$ cluster cut off from the edge of the lateral face of $\alpha$-$TiCl_3$.

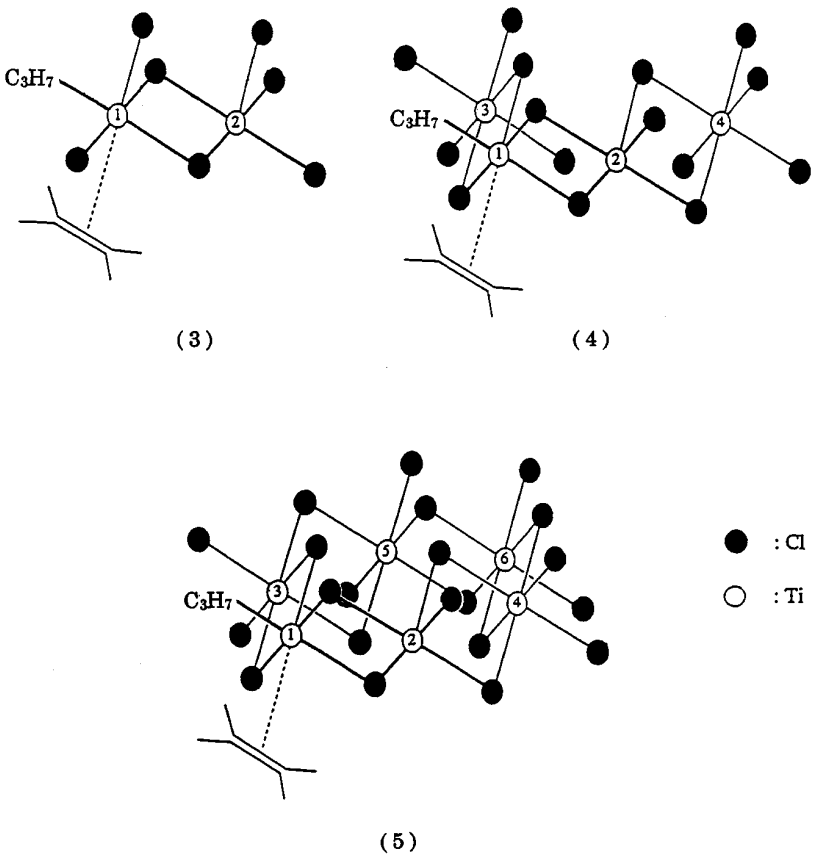


Figure 3. $O_h$-$d^1$-propyl$Ti_{2n}$ clusters ($n = 1, 2, 3$): complexes (3), (4), and (5).

Table 1
Structures and energies of $d^0$-propyltitaniumchlorides

| Complex | $\gamma$-agostic form | non-agostic form/T.S. | $\beta$-agostic form |
|---|---|---|---|
| *$C_3H_7TiCl_4$* | | | |
| Ti–H (Å) | 2.923 | – | 2.364 |
| $C_\gamma$–H (Å) | 1.085 | 1.084 | 1.104 |
| $\angle C_\alpha C_\beta C_\gamma$ (deg) | 112.6 | 109.5 | 111.6 [a] |
| $\angle TiC_\alpha C_\beta$ (deg) | 111.8 | 103.0 | 95.2 |
| $\angle ClTiC_\alpha$ (deg) | 138.1 | 131.2 | 136.1 |
| total energy (au) [b] | −2794.09963 | −2794.10059 [c] | −2794.10066 |
| relative energy (kcal/mol) | 0.0 | −0.60 | −0.65 |
| *$C_3H_7TiCl_2$* | | | |
| Ti–H (Å) | 2.246 | 2.144 | 2.075 |
| $C_\gamma$-H (Å) | 1.105 | 1.134 | 1.146 |
| $\angle C_\alpha C_\beta C_\gamma$ (deg) | 116.4 | 112.8 | 111.7 |
| $\angle TiC_\alpha C_\beta$ (deg) | 87.1 | 85.9 | 87.3 |
| $\angle ClTiC_\alpha$ (deg) | 105.1 | 104.9 | 105.4 |
| total energy (au) [b] | −1879.00808 | −1879.00024 [d] | −1879.00061 |
| relative energy (kcal/mol) | 0.0 | 4.9 | 4.7 |

[a] $\angle C_\alpha C_\beta$ H agostic.
[b] RHF.
[c] Non-agostic form.
[d] T.S.

enantiomeric active sites, *d* and *l*, which are composed of Ti ① and ③, and Ti ② and ④, respectively, are linked together at the edge. The titanium atom of the active center is Ti ① or Ti ②.

Here we employed the $O_h$-$d^1$-propyl$Ti_{2n}$ clusters ($n = 1, 2, 3$) as an active site model on the $TiCl_3$ crystalline surface. They are shown in figure 3.

### 3.2. Structures of propyltitaniumchlorides

In the case of $d^0[C_3H_7TiX_2]^+$ (X: Cp, Cl), it has already been reported that the first product of the ethylene insertion is a $\gamma$-H agostic propyltitanium. It is isomerized to the $\beta$-H agostic form spontaneously or by the attacking of the next incoming ethylene, and so the structure of alkyltitaniums is the $\beta$-H agostic form at the beginning of the second insertion [8]. We determined the structures of the $\gamma$- and $\beta$-H agostic forms of $O_h$-$d^0[C_3H_7TiCl_4]^-$ and $T_d$-$d^0[C_3H_7TiCl_2]^+$ by ab initio calculations. The results are summarized in table 1. The structures of these species are shown in figure 4. In the case of $O_h$-$d^0$-$[C_3H_7TiCl_4]^-$, the $\beta$-H agostic form and the non-agostic form are slightly more stable than the $\gamma$-H agostic form. Since the distance between the Ti atom and the agostic hydrogen is long, and that between the $C_\gamma$ atom and the hydrogen is almost the same as an ordinary carbon–hydrogen bond in length in the $\gamma$-H agostic form, the $\gamma$-H agostic interaction should be weak in the $O_h$-complex. An isomerization from the $\gamma$-H agostic form to the $\beta$-H agostic or the non-agostic form is suggested to be favorable. In the case of $T_d$-$d^0$-$[C_3H_7TiCl_2]^+$, the $\beta$-H agostic form is less stable than the $\gamma$-H agostic form; however, as the activation energy

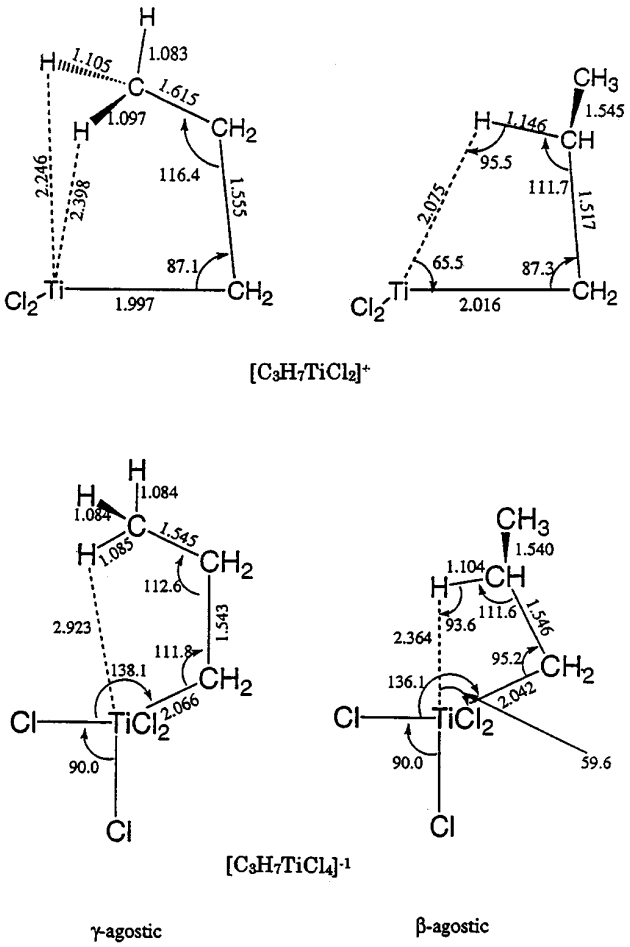


Figure 4. Structures of $\gamma$- and $\beta$-H agostic forms of $[C_3H_7TiCl_4]^-$ and $[C_3H_7TiCl_2]^+$.

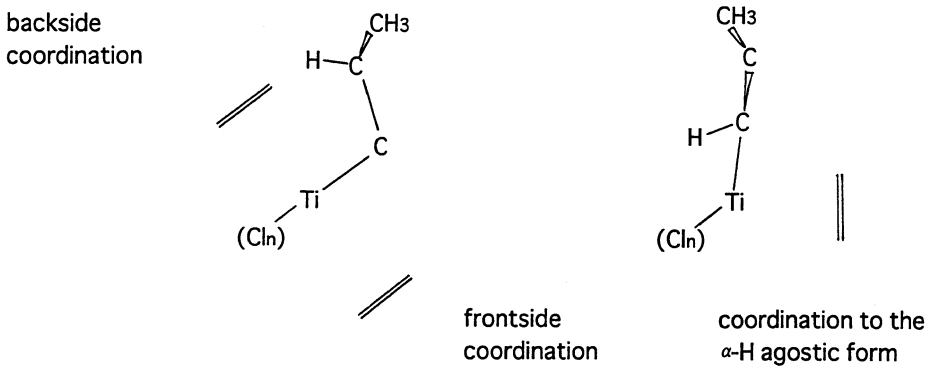


Figure 5. A schematic illustration of ethylene coordination to the $\beta$-H agostic propyltitanium complex.

of the isomerization from the $\gamma$-H agostic form to the $\beta$-H agostic form is small, the isomerization is also suggested to be possible.

### *3.3. Coordination of ethylene*

As described by Lohrenz et al. [8], there are three cases of ethylene coordination to the $\beta$-H agostic propyltitaniums: (1) frontside coordination, (2) backside coordination, and (3) frontside coordination with the isomerization of the $\beta$-H agostic form to the $\alpha$-H agostic form. They are schematically illustrated in figure 5.

As the incoming ethylene approaches, the propyl group has to move around the central Ti atom in the coordination plane in order to prepare the ethylene coordination space. From the fact that $\beta$-H agostic $d^0$-$[C_3H_7TiCl_4]^-$ (1) has two $Cl^-$ ligands in the ethylene coordination plane, while $\beta$-H agostic $d^0$-$[C_3H_7TiCl_2]^+$ (2) has no $Cl^-$ ligand in the coordination plane, it is supposed that this rotation is facile in the propyltitanium complex (2), whereas it is difficult in the propyltitanium complex (1). We examined the possibility of ethylene coordination to these two complexes by extended Hückel MO calculation. The structures of the complexes were determined by referring to the ab initio calculations described above. The detailed results and discussion are given in appendix 2.

The results are summarized in scheme 1.

Therefore, it is suggested that the complex (1)/olefin system ($O_h$-complex) is more suitable for getting the polymers with a higher molecular weight and a higher stereospecificity than the complex (2)/olefin system ($T_d$-complex).

### *3.4. Ethylene insertion*

The model $d^1$-$O_h$-propyl-$Ti_{2n}$ clusters ($n = 1, 2, 3$), employed here as the models of an active site on the $TiCl_3$ crystalline surface, have already been shown in figure 3. We have examined the ethylene coordinated state in each of these model systems.

#### *3.4.1. PIO analysis*

Eigenvalues of PIOs in the models, the MO components of PIO-1 and PIO-2, and the AO components of PIO-1 and PIO-2 are summarized in tables 2, 3, and 4, respectively.

We obtained twelve PIOs, PIO-1 to PIO-12. Eigenvalues shown in table 2 tell us that PIO-1 and PIO-2 have much lager contribution to the interaction relative to ten other orbital pairs. This is reasonable, because

complex (1)
- frontside $C_2H_4$ coordination; difficult
- backside $C_2H_4$ coordination; difficult
- isomerization to
  - non-agostic form $C_2H_4$ coordination (chain termination); rather difficult
  - $\alpha$-H agostic form $C_2H_4$ coordination (second insertion); facile,

complex (2)
- frontside $C_2H_4$ coordination (chain termination); possible
- backside $C_2H_4$ coordination (chain termination); possible
- isomerization to $\alpha$-H agostic form and $C_2H_4$ coordination (second insertion); possible.

Scheme 1.

Table 2
Eigenvalues of PIOs of the ethylene coordinated state of the model systems

| Model system | | PIO-1 | PIO-2 | PIO-3 | PIO-4 | PIO-5 | PIO-6 | ... | PIO-12 |
|---|---|---|---|---|---|---|---|---|---|
| $[C_3H_7Ti_2Cl_7]^{2-}$ (3)/ $C_2H_4$ | | 0.757 | 0.149 | 0.066 | 0.048 | 0.038 | 0.016 | ... | 0.000 |
| $[C_3H_7Ti_4Cl_{15}]^{4-}$ (4)/ $C_2H_4$ | | 0.765 | 0.154 | 0.066 | 0.052 | 0.048 | 0.016 | ... | 0.000 |
| $[C_3H_7Ti_6Cl_{21}]^{4-}$ (5)/ $C_2H_4$ | | 0.778 | 0.155 | 0.067 | 0.051 | 0.042 | 0.017 | ... | 0.000 |
| $[C_3H_7TiCl_2]$ (6)/ $C_2H_4$ | $\alpha$ spin | 0.172 | 0.062 | 0.010 | 0.009 | 0.008 | 0.002 | ... | 0.000 |
| | $\beta$ spin | 0.067 | 0.030 | 0.009 | 0.009 | 0.004 | 0.002 | ... | 0.000 |

two bonds are formed in the insertion process. Tables 3 and 4 tell us that the main component of the ethylene part in PIO-1 is the LUMO ($\pi^*$ orbital) in all the model systems. This signifies that PIO-1 represents electron delocalization from the occupied orbitals of the propyltitanium complexes which are mainly composed of the Ti ① $d(t_{2g})$ orbital (see table 4), to the ethylene $\pi^*$ orbital. In contrast, the main components of the ethylene part in PIO-2 are the HOMO and $\psi_1$ occupied orbital, and those of the propyltitanium complex part in PIO-2 are the mixtures of some occupied orbitals and some unoccupied orbitals. This indicates that PIO-2 represents electron delocalization from the ethylene $\pi$ orbital to the unoccupied orbitals of the propyltitanium complexes which are composed of Ti ① $d(e_g)$ orbital and $C_\alpha$ p orbital, but a repulsive interaction intervenes between the occupied $C_{\alpha,\beta}$ 2s and H 1s orbitals of ethylene and the occupied Cl p orbitals of the catalyst.

These results are compactly shown with the contour maps of PIO-1 and PIO-2 of the model systems in figure 6.

*3.4.2. Reactivity index (RI) of the model systems*

The PIO analysis is useful to understand the nature of chemical interactions in a qualitative sense. The next thing to do is to estimate the strength of the chemical interactions (reactivities) quantitatively by using the LFO scheme.

From the results of the PIO analysis on the $[C_3H_7Ti_2Cl_7]^{2-}$ (3)/$C_2H_4$ system, which is used as a control, we determined a reference orbital $\delta_r$ as follows:

for the occupied orbital (oc) space of propyltitanium complexes:

$$(\delta_r)_{\mathrm{A\,oc}} = 0.20\mathrm{C}_\alpha\,\mathrm{p}_x - 0.85\mathrm{Ti}\,\mathrm{d}_{xz} - 0.20\mathrm{Ti}\,\mathrm{d}_{xy}\,; \quad (13)$$

for the unoccupied orbital (unoc) space of the ethylene molecule:

$$(\delta_r)_{\mathrm{B\,unoc}} = 0.82\mathrm{C}_\alpha\,\mathrm{p}_x - 0.82\mathrm{C}_\beta\,\mathrm{p}_x\,; \quad (14)$$

for the unoccupied space of propyltitanium complexes:

$$(\delta_r)_{\mathrm{A\,unoc}} = -0.21\mathrm{C}_\alpha\,\mathrm{p}_x + 0.45\mathrm{Ti}\,\mathrm{d}_{x^2-y^2} + 0.17\mathrm{Ti}\,\mathrm{d}_{z^2}\,; \quad (15)$$

Table 3
LCMO representation of PIO-1 and PIO-2 of the ethylene coordinated state of the model systems

| | | |
|---|---|---|
| *PIO-1* | | |
| $\underline{C_2H_4\ \text{part}}$ | | $1.00\psi_7(\mathrm{LUMO}) + \ldots$ |
| $\overline{[C_3H_7Ti_2Cl_7]^{2-}\ \text{part}}$ | | $-0.20\phi_{38} + 0.79\phi_{39}(\mathrm{HOMO}) + 0.48\phi_{42} + 0.28\phi_{43} + \ldots$ |
| $\underline{C_2H_4\ \text{part}}$ | | $1.00\psi_7(\mathrm{LUMO}) + \ldots$ |
| $\overline{[C_3H_7Ti_4Cl_{15}]^{4-}\ \text{part}}$ | | $-0.20\phi_{70} - 0.24\phi_{71} + 0.53\phi_{72}(\mathrm{HOMO}) + 0.58\phi_{74} + 0.46\phi_{75} + \ldots$ |
| $\underline{C_2H_4\ \text{part}}$ | | $1.00\psi_7(\mathrm{LUMO}) + \ldots$ |
| $\overline{[C_3H_7Ti_6Cl_{21}]^{4-}\ \text{part}}$ | | $-0.19\phi_{94} - 0.20\phi_{95} + 0.20\phi_{96}(\mathrm{HOMO}-1) + 0.57\phi_{98}(\mathrm{LUMO}) - 0.47\phi_{100} - 0.31\phi_{101} - 0.44\phi_{103} - 0.16\phi_{104} + \ldots$ |
| $C_2H_4$ part | $\alpha$ spin | $0.98\psi_7(\mathrm{LUMO}) + \ldots$ |
| | $\beta$ spin | $0.99\psi_6(\mathrm{HOMO}) + \ldots$ |
| $[C_3H_7TiCl_2]$ | $\alpha$ spin | $-0.49\phi_{19}(\mathrm{SOMO}) - 0.81\phi_{20} + 0.25\phi_{24} + \ldots$ |
| | $\beta$ spin | $-0.95\phi_{19}(\mathrm{SOMO}) + 0.24\phi_{20} + \ldots$ |
| *PIO-2* | | |
| $\underline{C_2H_4\ \text{part}}$ | | $-0.63\psi_1 - 0.74\psi_6(\mathrm{HOMO}) + \ldots$ |
| $\overline{[C_3H_7Ti_2Cl_7]^{2-}\ \text{part}}$ | | $0.35\phi_1 - 0.42\phi_{26} - 0.28\phi_{45}(\mathrm{LUMO}+5) - 0.28\phi_{46} + 0.26\phi_{55} + \ldots$ |
| $\underline{C_2H_4\ \text{part}}$ | | $0.57\psi_1 + 0.79\psi_6(\mathrm{HOMO}) + \ldots$ |
| $\overline{[C_3H_7Ti_4Cl_{15}]^{4-}\ \text{part}}$ | | $0.25\phi_1 + 0.25\phi_3 - 0.25\phi_{45} - 0.24\phi_{80}(\mathrm{LUMO}+8) + 0.24\phi_{83} + 0.33\phi_{84} + \ldots$ |
| $\underline{C_2H_4\ \text{part}}$ | | $-0.58\psi_1 - 0.79\psi_6(\mathrm{HOMO}) + \ldots$ |
| $\overline{[C_3H_7Ti_6Cl_{21}]^{4-}\ \text{part}}$ | | $-0.26\phi_3 + 0.23\phi_{66} - 0.16\phi_{106}(\mathrm{LUMO}+8) + 0.14\phi_{108} - 0.14\phi_{109} - 0.21\phi_{113} - 0.33\phi_{114}$ |
| $C_2H_4$ part | $\alpha$ spin | $-0.99\psi_6(\mathrm{HOMO}) + \ldots$ |
| | $\beta$ spin | $0.54\psi_2 + 0.22\psi_5 - 0.80\psi_7(\mathrm{LUMO}) + \ldots$ |
| $[C_3H_7TiCl_2]$ | $\alpha$ spin | $-0.84\phi_{19}(\mathrm{SOMO}) + 0.48\phi_{20} - 0.16\phi_{21} + \ldots$ |
| | $\beta$ spin | $-0.20\phi_{15} + 0.27\phi_{16} - 0.18\phi_{17} + 0.83\phi_{18}(\mathrm{SOMO}-1) + \ldots$ |

Table 4
LCAO representation of PIO-1 and PIO-2 of the ethylene coordinated state of the model systems

| | | |
|---|---|---|
| *PIO-1* | | |
| $C_2H_4$ part | | $0.82C_\alpha p_x - 0.82C_\beta p_x + \ldots$ |
| $[C_3H_7Ti_2Cl_7]^{2-}$ part | | $0.20C_\alpha p_x - 0.85Ti_① d_{xz} - 0.20Ti_① d_{xy} + 0.26Cl_{13} p_y + 0.36Ti_② d_{xz} + 0.37Ti_② d_{xy} + \ldots$ |
| $C_2H_4$ part | | $-0.82C_\alpha p_x + 0.82C_\beta p_x + \ldots$ |
| $[C_3H_7Ti_4Cl_{15}]^{4-}$ part | | $-0.21C_\alpha p_x + 0.87Ti_① d_{xz} + 0.28Ti_① d_{yz} - 0.17Ti_① d_{xy} - 0.20Cl_{13} p_y - 0.18Ti_② d_{xz}$ $-0.19Ti_② d_{xy} - 0.18Ti_③ d_{yz} - 0.17Ti_③ d_{xy} + \ldots$ |
| $C_2H_4$ part | | $-0.82C_\alpha p_x + 0.82C_\beta p_x + \ldots$ |
| $[C_3H_7Ti_6Cl_{21}]^{4-}$ part | | $-0.24C_\alpha p_x + 0.87Ti_① d_{xz} - 0.22Cl_{13} p_z - 0.38Ti_② d_{xy} + \ldots$ |
| $C_2H_4$ part | $\alpha$ spin | $0.82C_\alpha p_x - 0.79C_\beta p_x + \ldots$ |
| | $\beta$ spin | $-0.65C_\alpha p_x - 0.60C_\beta p_x + \ldots$ |
| $[C_3H_7TiCl_2]$ | $\alpha$ spin | $-0.21C_\alpha p_x + 0.26Tid_{x^2-y^2} + 0.98Tid_{xz} + \ldots$ |
| | $\beta$ spin | $0.18C_\alpha p_x - 0.26Ti4s + 0.79Tid_{x^2-y^2} + 0.50Tid_{z^2} + \ldots$ |
| *PIO-2* | | |
| $C_2H_4$ part | | $-0.22C_\alpha 2s - 0.46C_\alpha p_x - 0.21H_1 1s - 0.23H_2 1s + 0.16C_\beta 2s - 0.47C_\beta p_x - 0.17H_3 1s - 0.17H_4 1s + \ldots$ |
| $[C_3H_7Ti_2Cl_7]^{2-}$ part | | $-0.21C_\alpha p_x + 0.45Ti_① d_{x^2-y^2} + 0.17Ti_① d_{z^2} - 0.37Cl_{12} p_x + 0.36Cl_{13} 3s - 0.56Cl_{13} p_x - 0.25Cl_{14} p_x - 0.21Cl_{15} p_x + \ldots$ |
| $C_2H_4$ part | | $0.21C_\alpha 2s + 0.48C_\alpha p_x + 0.19H_1 1s + 0.21H_2 1s + 0.16C_\beta 2s + 0.51C_\beta p_x + 0.14H_3 1s + 0.13H_4 1s + \ldots$ |
| $[C_3H_7Ti_4Cl_{15}]^{4-}$ part | | $0.16C_\alpha p_x - 0.52Ti_① d_{x^2-y^2} - 0.22Ti_① d_{z^2} + 0.37Cl_{12} p_x - 0.31Cl_{13} 3s - 0.56Cl_{13} p_x + 0.23Cl_{14} p_x + \ldots$ |
| $C_2H_4$ part | | $0.22C_\alpha 2s + 0.49C_\alpha p_x + 0.19H_1 1s + 0.21H_2 1s + 0.16C_\beta 2s + 0.50C_\beta p_x + 0.15H_3 1s + 0.14H_4 1s + \ldots$ |
| $[C_3H_7Ti_6Cl_{21}]^{4-}$ part | | $-0.18C_\alpha p_x + 0.51Ti_① d_{x^2-y^2} + 0.21Ti_① d_{z^2} - 0.37Cl_{12} p_x + 0.31Cl_{13} 2s - 0.53Cl_{13} p_x - 0.24Cl_{14} p_x - 0.17Cl_{15} p_x + \ldots$ |
| $C_2H_4$ part | $\alpha$ spin | $-0.61C_\alpha p_x - 0.64C_\beta p_x + \ldots$ |
| | $\beta$ spin | $-0.63C_\alpha p_x - 0.25C_\beta p_z + 0.67C_\beta p_x - 0.26H_3 1s - 0.26H_4 1s + \ldots$ |
| $[C_3H_7TiCl_2]$ | $\alpha$ spin | $0.17C_\alpha p_z + 0.31C_\alpha p_x + 0.69Tid_{x^2-y^2} + 0.53Tid_{z^2} - 0.22Tid_{xz} + \ldots$ |
| | $\beta$ spin | $0.19C_\alpha 2s - 0.47C_\alpha p_z - 0.50C_\alpha p_x + 0.30Tid_{x^2-y^2} - 0.18Tid_{z^2} - 0.25Tid_{xz} + \ldots$ |

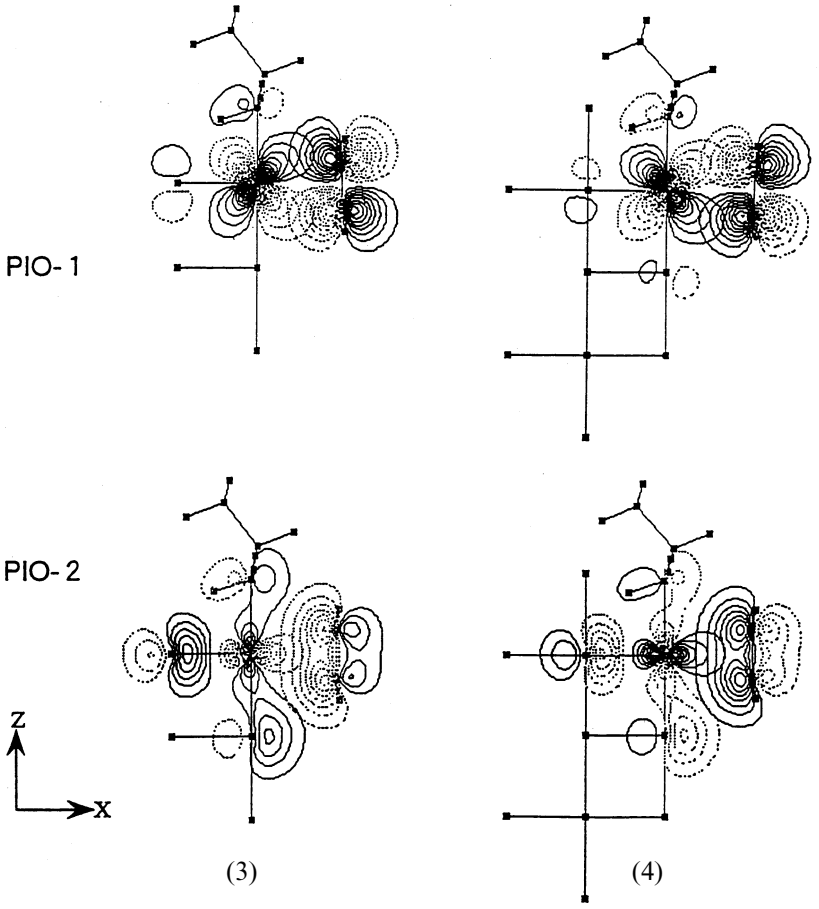


Figure 6. Contour maps of PIO-1 and PIO-2 of the ethylene coordinated state of complexes (3) and (4).

for the occupied space of the ethylene molecule:

$$(\delta_r)_{\mathrm{B\,oc}} = 0.22\mathrm{C}_\alpha\,2\mathrm{s} - 0.46\mathrm{C}_\alpha\,\mathrm{p}_x - 0.21\mathrm{H}_1\,1\mathrm{s} - 0.23\,\mathrm{H}_2 1\mathrm{s} - 0.16\mathrm{C}_\alpha\,2\mathrm{s} - 0.47\mathrm{C}_\beta\,\mathrm{p}_x - 0.17\mathrm{H}_3 1\mathrm{s} - 0.17\mathrm{H}_4\,1\mathrm{s}\,. \quad (16)$$

Nucleophilicity ($\lambda_{\mathrm{oc}}$) and electrophilicity ($\lambda_{\mathrm{unoc}}$) of the propyltitanium complexes (A) and the ethylene molecule (B), and a reactivity index (RI) for the ethylene insertion are summarized in table 5. The difference of RI of the propyltitanium complexes, (3), (4), and (5) are not large. It is sufficient to employ $Ti_4$ cluster (4) as a model of the active site on the $TiCl_3$ crystalline surface.

### 3.4.3. *Comparison between $TiCl_3$ catalyst and metallocene type catalyst*

We employed $T_d$-$d^1$-$[C_3H_7TiCl_2]$ (6) as a model of metallocene type catalyst. We have assumed that the geometry is the same as that of the complex (2). The results of PIO analysis and LFO calculation on the model are also summarized in tables 2, 3, 4, and 5. As the complex (6) has odd numbers of electrons, the results of $\alpha$ spin electrons and $\beta$ spin electrons are obtained separately. The PIO analysis of $\alpha$ spin electrons of the complex (6)/ethylene system shows that the PIO-1 represents electron delocalization from the occupied Ti $d_{xz}$ orbital to the ethylene $\pi^*$ orbital. This PIO-1 is basically the same as the PIO-1 of $O_h$-complex (3), (4), and (5)/ethylene systems. The PIO-2 represents electron delocalization from the $\pi$ orbital of the ethylene to the unoccupied Ti d($e_g$) orbital. Since the complex (6) has no Cl anion in the ethylene coordination plane, electron delocalization takes place more smoothly in the complex (6)/ethylene system than in the $O_h$-complexes/ethylene systems. The PIO analysis of $\beta$ spin electrons of the system shows that the PIO-1 represents electron delocalization from the $\pi$ orbital of the ethylene to the unoccupied Ti d($e_g$) orbitals, while PIO-2 represents electron delocalization from the occupied orbital (SOMO-1 that is HOMO) which is mainly composed of $C_\alpha$ p orbitals, to the ethylene $\pi^*$ orbital. A small overlap repulsion between the propyl $C_\alpha$ 2s orbital and the ethylene $C_\alpha$ $p_z$ and H 1s orbitals is included in this orbital. The overlap repulsion is small because there is no Cl anion in the ethylene coordination plane. These results described above are understood easily by referring to the contour maps of PIO-1 and PIO-2, shown in figure 7.

Referring to PIO-1 and PIO-2 of the complex (6)/ethylene system, we determined the reference orbitals of the fragment A (the complex (6)) and the fragment B (ethylene) for the $\alpha$ spin and $\beta$ spin electrons of the occupied space and the unoccupied space, respectively, as follows:

for $\alpha$ spin electrons:

$$(\delta_r)_{\mathrm{A\,oc}} = -0.21\mathrm{C}_\alpha\,\mathrm{p}_x + 0.26\mathrm{Ti}\,\mathrm{d}_{x^2-y^2} + 0.98\mathrm{Ti}\,\mathrm{d}_{xz}\,, \quad (17)$$

$$(\delta_r)_{\mathrm{B\,unoc}} = 0.82\mathrm{C}_\alpha\,\mathrm{p}_x - 0.79\mathrm{C}_\beta\,\mathrm{p}_x\,, \quad (18)$$

$$(\delta_r)_{\mathrm{A\,unoc}} = 0.17\mathrm{C}_\alpha\,\mathrm{p}_z + 0.31\mathrm{C}_\alpha\,\mathrm{p}_x + 0.69\mathrm{Ti}\,\mathrm{d}_{x^2-y^2} + 0.53\mathrm{Ti}\,\mathrm{d}_{z^2} - 0.22\mathrm{Ti}\,\mathrm{d}_{xz}\,, \quad (19)$$

$$(\delta_r)_{\mathrm{B\,oc}} = -0.61\mathrm{C}_\alpha\,\mathrm{p}_x - 0.64\mathrm{C}_\beta\,\mathrm{p}_x\,; \quad (20)$$

for $\beta$ spin electrons:

$$(\delta_r)_{\mathrm{A\,unoc}} = 0.18\mathrm{C}_\alpha\,\mathrm{p}_x - 0.26\mathrm{Ti}\,4\mathrm{s} + 0.79\mathrm{Ti}\,\mathrm{d}_{x^2-y^2} + \mathrm{Ti}\,\mathrm{d}_{z^2}\,, \quad (21)$$

$$(\delta_r)_{\mathrm{B\,oc}} = -0.65\mathrm{C}_\alpha\,\mathrm{p}_x - 0.60\mathrm{C}_\beta\,\mathrm{p}_x\,, \quad (22)$$

$$(\delta_r)_{\mathrm{A\,oc}} = -0.47\mathrm{C}_\alpha\,\mathrm{p}_z - 0.50\mathrm{C}_\alpha\,\mathrm{p}_x + 0.30\mathrm{Ti}\,\mathrm{d}_{x^2-y^2} - 0.18\mathrm{Ti}\,\mathrm{d}_{z^2} - 0.25\mathrm{Ti}\,\mathrm{d}_{xz}\,, \quad (23)$$

Table 5
LFO energies, nucleophilicity and electrophilicity of ethylene and reactivity index (RI) for ethylene insertion of model systems

| Model system | | $\lambda_{\mathrm{oc}}$ (eV) | Nucleophilicity [a] | $\lambda_{\mathrm{unoc}}$ (eV) | Electrophilicity [b] | RI [c] |
|---|---|---|---|---|---|---|
| $O_h$-$[C_3H_7Ti_2Cl_7]^{2-}$ (3) | | −10.11 | 0.55 | −0.03 | 0.08 | 0.63 |
| $O_h$-$[C_3H_7Ti_4Cl_{15}]^{4-}$ (4) | | −10.78 | 0.40 | −0.09 | 0.08 | 0.48 |
| $O_h$-$[C_3H_7Ti_6Cl_{21}]^{4-}$ (5) | | −10.51 | 0.45 | −0.13 | 0.08 | 0.53 |
| $C_2H_4$ | | −13.20 | – | −8.30 | – | – |
| $T_d$-$[C_3H_7TiCl_2]$ (6) | $\alpha$ spin | −9.70 | 0.71 | −8.67 | 0.23 | 0.47 [d] |
| | $\beta$ spin | −13.53 | 0.16 | −10.18 | 0.33 | 0.25 [d] |
| | | | | | | $\sum$0.72 |
| $C_2H_4$ | $\alpha$ spin | −13.20 | – | −8.30 | – | – |
| | $\beta$ spin | −13.20 | – | −7.35 | – | – |

[a] $1/(\lambda_{\mathrm{B\,unoc}} - \lambda_{\mathrm{A\,oc}})$.
[b] $1/(\lambda_{\mathrm{A\,unoc}} - \lambda_{\mathrm{B\,oc}})$.
[c] Nucleophilicity + electrophilicity.
[d] $1/2 \times$ (nucleophilicity + electrophilicity).

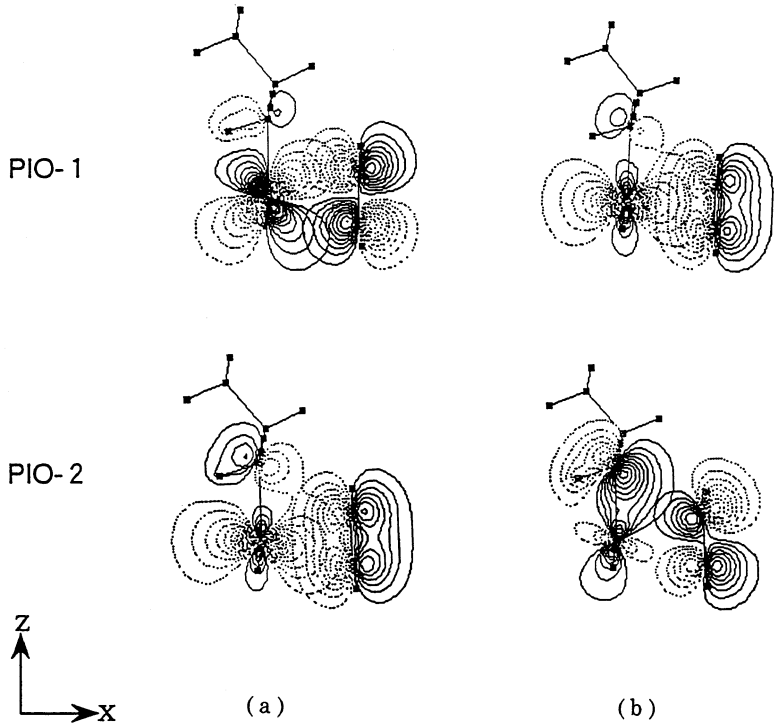


Figure 7. Contour maps of PIO-1 and PIO-2 of the ethylene coordinated state of complex (6). (a) $\alpha$ spin part and (b) $\beta$ spin part.

$$(\delta_r)_{\mathrm{B\,unoc}} = -0.63\mathrm{C}_\alpha\,\mathrm{p}_x - 0.25\mathrm{C}_\beta\,\mathrm{p}_z + 0.67\mathrm{C}_\beta\,\mathrm{p}_x - 0.26\mathrm{H}_3\,1\mathrm{s} - 0.26\mathrm{H}_4\,1\mathrm{s}\,. \quad (24)$$

The calculated results are shown in table 6. Electrophilicities of the $\alpha$ and $\beta$ spin parts of the $T_d$-complex (6) are seen to be markedly large owing to the absence of Cl anions in the ethylene coordination plane. Nucleophilicity of the $\beta$ spin part of the complex (6) is small because there is no electron in the d orbitals of the Ti atom. The value of the reactivity index, 0.72, an average of RI for the $\alpha$ spin part and that for the $\beta$ spin part, is higher than those of the $O_h$-complexes (3), (4), and (5). In other words, the $O_h$-complexes are enhanced in catalytic activity by making $Ti_{2n}$ clusters, which have even numbers of Ti d electrons, on the $TiCl_3$ crystalline surface.

Table 6
Extended Hückel parameters

| Orbital | *Hii* (eV) | $\zeta 1$ | $\zeta 2$ | C1 | C2 |
|---|---|---|---|---|---|
| H1s | −13.60 | 1.30 | | | |
| C2s | −21.40 | 1.625 | | | |
| C2p | −11.40 | 1.625 | | | |
| Cl3s | −30.00 | 2.033 | | | |
| Cl3p | −15.00 | 2.033 | | | |
| Ti4s | −8.97 | 1.075 | | | |
| Ti4p | −5.44 | 0.675 | | | |
| Ti3d | −10.81 | 4.553 | 1.40 | 0.4206 | 0.7389 |

## 4. Conclusion

We have examined $O_h$-propyltitaniumchlorides and $T_d$-propyltitaniumchlorides as active site models of heterogeneous $TiCl_3$ type catalysts and metallocene catalysts, respectively. In the case of $TiCl_3$ catalysts, an active site is located on the edge of the lateral face of the $TiCl_3$ crystalline surface, and therefore, the route of the ethylene attack for coordination to the active site from the basal face of the $TiCl_3$ crystal is blocked by Cl anions located on the basal face. The possible route for the approach of an incoming ethylene is limited to from the lateral face. In the case of metallocene catalysts, such a constraint does not appear.

As the propyl group of the active site exists in the $\beta$-H agostic resting state, there are three cases of ethylene coordination: (1) the frontside coordination, (2) the backside coordination, and (3) the frontside coordination with isomerization of the $\beta$-H agostic form to the $\alpha$-H agostic form. In the case of $TiCl_3$ catalysts, cases (1) and (2) are difficult to take place, and case (3) is facile, while all the three cases are possible in metallocene catalysts.

The active site of $TiCl_3$ catalysts is presented properly by $O_h$-$d^1$-alkyl-$Ti_4$-chloride. Since no Cl anion is located in the ethylene insertion plane in the case of metallocene catalysts, they should be superior to $TiCl_3$ catalysts in catalytic activity. The low reactivities of $TiCl_3$ catalysts are removed considerably by making $Ti_{2n}$ clusters, which have even numbers of Ti d electrons in the case of $TiCl_3$ catalysts.

The results discussed above suggest that heterogeneous catalysts are suitable for highly stereospecific polymerization, whereas metallocene catalysts are very active and are suitable for copolymerization.

## Acknowledgement

We thank Professor H. Fujimoto for helpful advice and Sumitomo Chemical Co. Ltd. for permission to publish.

## Appendix 1

Coulomb integrals and orbital exponents are listed in table 6.

## Appendix 2

The changes in total energies (eV) of propyltitaniumchlorides and propyltitaniumchlorides/ethylene $\pi$-complexes with rotation around the central Ti atom in the coordination plane ($\theta$) and around the Ti–$C_\alpha$ bond ($\phi$) are summarized in table 7. In the case of the complex (1), ethylene coordination is impossible both from the frontside and from the backside of the $\beta$-H agostic bond, because the rotation of the propyl group in the coordination plane is hindered by the two Cl anions located in the plane. The isomerization of the $\beta$-H agostic form to the non-agostic form or the $\alpha$-H agostic form is necessary for the ethylene coordination. Table 7 tells us that the change in the total energy of the ethylene $\pi$-complex in going to the $\alpha$-H agostic form and to the non-agostic form are −1173.91 and −1172.22 eV, respectively, and hence ethylene coordination to the $\alpha$-H agostic form is more favorable than that to the non-agostic form. The transformation of ethylene $\pi$-complex to the $\alpha$-H agostic form gives the starting intermediate of ethylene insertion and that of the ethylene $\pi$-complex to the non-agostic form from the the frontside yields the starting intermediate of chain termination with hydrogen exchange. It is suggested, therefore, that the complex (1) / olefin system ($O_h$-complex) is suitable for getting the polymers with a higher molecular weight and a higher stereospecificity. On the other hand, in the case of the complex (2), there is no Cl anion in the ethylene coordination plane, and therefore, there is enough space for the ethylene coordination in the plane. The stabilization arising from the transformation of the ethylene $\pi$-complex to the $\beta$-H agostic form from the frontside and from the backside, and that to the $\alpha$-H agostic form have been calculated to be almost the same, −873.32, −873.59, and −873.73 eV,

Table 7
Changes in total energies (eV) of propyltitaniumchlorides and propyltitaniumchlorides/ethylene $\pi$-complexes with rotation around the central Ti atom in the coordination plane ($\theta$) and around the Ti–$C_\alpha$ bond ($\phi$)

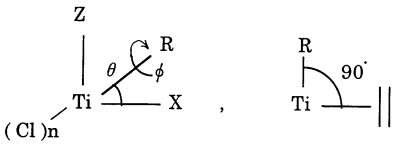


| Complex | (1) [a] | (1)/$C_2H_4$ | (2) [a] | (2)/$C_2H_4$ |
|---|---|---|---|---|
| *frontside $C_2H_4$ attack to the $\beta$-H agostic form* | | | | |
| $\theta$: 90° | −960.63 [b] | −1166.70 [b] | −658.97 | −873.32 |
| 105° | −959.78 [b] | −1172.22 [b] | | |
| 120° | −956.00 [b] | −1169.62 [b] | | |
| *backside $C_2H_4$ attack to the $\beta$-H agostic form* | | | | |
| $\theta$: 0° | | | −658.92 | −872.52 |
| 15° | | | −658.92 | −873.03 |
| 30° | | | −658.90 | −873.41 |
| 45° | −961.25 | −1154.91 | −658.88 | −873.52 |
| 60° | −960.32 | −1166.00 | −658.83 | −873.59 |
| 75° | −956.83 | −1168.87 | −658.75 | −873.56 |
| 90° | −951.65 | −1167.24 | −658.57 | −873.42 |
| *$C_2H_4$ attack to the $\alpha$-H agostic form* | | | | |
| $\phi$: 120°, $\theta$: 45° | | | −658.64 | −873.60 |
| 60° | −961.38 | −1167.02 | −658.64 | −873.70 |
| 75° | −961.14 | −1173.15 | −658.63 | −873.73 |
| 90° | −960.01 | −1173.91 | −658.58 | −873.70 |

[a] (1): $d^0$-$[C_3H_7TiCl_4]^-$; (2): $d^0$-$[C_3H_7TiCl_2]^+$.
[b] Nonagostic form.

respectively. Therefore, these three types of ethylene coordination should occur in the complex (2). It is suggested that the polymers produced in the complex (2)/olefin system ($T_d$-complex) should have a lower molecular weight and a lower stereospecificity.

## References


[1] H. Sinn and W. Kaminsky, Adv. Organometal. Chem. 18 (1980) 99.

[2] P. Cossee, J. Catal. 3 (1964) 80.

[3] P. Novaro, E. Blaisten-Barojas, E. Clementi, G. Giunch and M.E. Ruizvizcaya, J. Chem. Phys. 68 (1978) 2337.

[4] D.R. Armstrong, P.G. Perkins and J.J.P. Stewart, J. Chem. Soc. Dalton Trans. (1972) 1972.

[5] C.A. Jolly and D.S. Marynick, J. Am. Chem. Soc. 111 (1989) 7968.

[6] H. Kawaruma-Kuribayashi, N. Koga and K. Morokuma, J. Am. Chem. Soc. 114 (1992) 2359.

[7] T. Yoshida, N. Koga and K. Morokuma, Organometallics (1995) 746.

[8] J.C.W. Lohrenz, T.K. Woo, L. Fan and T. Ziegler, J. Organometal. Chem. 497 (1995) 91;
J.C.W. Lohrenz, T.K. Woo and T. Ziegler, J. Am. Chem. Soc. 117 (1995) 12793.

[9] H. Kawamura-Kuribayashi, N. Koga and K. Morokuma, J. Am. Chem. Soc. 114 (1992) 8687;
T. Yoshida, N. Koga and K. Morokuma, Organometallics (1996) 766.

[10] H. Fujimoto, N. Koga and K. Fukui, J. Am. Chem. Soc. 103 (1981) 7452;
H. Fujimoto, N. Koga and I. Hataue, J. Phys. Chem. 88 (1984) 3539;
H. Fujimoto, T. Yamasaki, H. Mizutani and N. Koga, J. Am. Chem. Soc. 107 (1985) 6157;
H. Fujimoto, Acc. Chem. Res. 20 (1987) 448.

[11] A. Shiga, H. Kawamura, T. Ebara, T. Sasaki and Y. Kikuzono, J. Organometal. Chem. 366 (1989) 95;
A. Shiga, H. Kawamura-Kuribayashi and T. Sasaki, J. Mol. Catal. 77 (1992) 135;
A. Shiga, H. Kawamura-Kuribayashi and T. Sasaki, J. Mol. Catal. 79 (1993) 95;
A. Shiga, H. Kawamura-Kuribayashi and T. Sasaki, J. Mol. Catal. A 98 (1995) 15.

[12] H. Fujimoto, Y. Mizutani and K. Iwase, J. Phys. Chem. 90 (1986) 2768;
H. Fujimoto, K. Hatakeyama, S. Kawasaki and Y. Oishi, J. Chem. Soc. Perkin Trans. II (1991) 989;
K. Omoto, Y. Sawada and H. Fujimoto, J. Am. Chem. Soc. 118 (1996) 1751.

[13] A. Shiga, J. Macromol. Sci. A34 (10), in press.

[14] J.A. Pople, M.J. Frisch, G.W. Trucks et al., GAUSSIAN 94, Revision C.3 (Gaussian Inc., Pittsburgh, PA, 1995).

[15] S. Huzinaga, J. Andzelm, M. Klobukowski, E. Radzio-Amdzelm, Y. Sasaki and H. Tatewaki, *Gaussian Basis Sets for Molecular Calculations* (Elsevier, Amsterdam, 1984).

[16] J.S. Binkley, J.A. Pople and W.J. Hehere, J. Am. Chem. Soc. 102 (1980) 939;
M.S. Gordon, J.S. Binkley, J.A. Pople, W.J. Pietro and W.J. Hehere, J. Am. Chem. Soc. 104 (1982) 2797.

[17] J. Howell, A. Rossi, D. Wallace, K. Haraki and R. Hoffmann, QCPE Program No. 344.

[18] H. Katsumi, Y. Kikuzono, M. Yoshida, A. Shiga and H. Fujimoto, Chem. Info. Comp. Sci. (Jpn.), Preprint, 12 (1989) 72.

[19] G. Natta, J. Polymer Sci. 34 (1959) 21;
G. Natta, P. Corradini and G. Allegra, J. Polymer Sci. 51 (1961) 399;
L.A.M. Rodriguez and H.M. van Looy, J. Polymer Sci. A-1 4 (1966) 1905;
T. Keii, *Kinetics of Ziegler–Natta Polymerization* (Kodanshya, Tokyo, 1972);
J. Boor Jr., *Ziegler–Natta Catalysts and Polymerization* (Academic Press, New York, 1979);
A. Shiga and T. Sasaki, Polymer Preprints, Japan 36 (1987) 190.